Journal of Nuclear Materials 386–388 (2009) 97–101

Contents lists available at ScienceDirect

Journal of Nuclear Materials

journal homepage: www.elsevier.com/locate/jnucmat

Molecular dynamics simulation of radiation damage in bcc tungsten

J. Fikar *, R. Schäublin

Ecole Polytechnique Fédérale de Lausanne (EPFL), Centre de Recherches en Physique des Plasmas, Association Euratom – Confédération Suisse, 5232 Villigen PSI, Switzerland

A B S T R A C T

Molecular dynamics simulations of collision cascades in pure tungsten are performed to assess the primary damage due to irradiation. For short-range interaction the universal potential is used [J.F. Ziegler, J.P. Biersack, U. Littmark, The Stopping and Range of Ions in Solids, Pergamon Press, 1985, p. 41], while for long-range interaction, three different embedded atom method potentials [M.W. Finnis, J.E. Sinclair, Phil. Mag. A 50 (1984) 45; G.J. Ackland, R. Thetford, Phil. Mag. A 56 (1987) 15; P.M. Derlet, D. Nguyen-Manh, S.L. Dudarev, Phys. Rev. B 76 (2007) 054107] are used, namely, Finnis–Sinclair, Ackland–Thetford and Derlet–Nguyen–Manh–Dudarev, the latter providing a more accurate formation energy for the ⟨1 1 0⟩ interstitial. The short-range and long-range potentials are smoothly connected. A new approach improving the reliability of such potential fits at short distances is presented. These potentials are then evaluated on the basis of displacement threshold, point defect formation and migration energies, thermal expansion and temperature of melting. Differences in the damage resulting from collision cascades are discussed.

1. Introduction

Due to its high melting point and good irradiation resistance tungsten is a promising candidate material for high temperature and irradiation applications, e.g. for the divertor armour of the future thermonuclear fusion reactors. The 14 MeV fusion neutron irradiation of metals produces atomic displacements which result in vacancies and interstitials. These point defects may form clusters such as cavities and dislocation loops and cause irradiation induced hardening and shift of the ductile to brittle transition temperature to higher values [5].

In this paper molecular dynamics (MD) simulations are used to study the influence of the tungsten empirical interatomic potential on the amount and type of radiation damage. Two existing potentials, namely Finnis–Sinclair and Ackland–Thetford [2,3], already studied in [6,7], overestimate the formation energy of the ⟨1 1 0⟩ interstitial. A new potential [4] was developed to solve this problem. The focus of this investigation is to evaluate this potential in the formation of radiation damage by displacement cascades in comparison to previously studied potentials.

2. Method

2.1. Simulation setup

The modified MD code MOLDY [8] is used to study the damage produced by self-irradiation in tungsten. The system sizes are chosen according to the primary knock-on atom (PKA) energy and the number of atoms ranges from 119,000 to 2 million. The chosen PKA directions are ⟨1 2 2⟩, ⟨1 3 3⟩, ⟨1 3 5⟩, and ⟨2 3 5⟩. For all simulations periodic boundary conditions and constant volume are used. Details can be found in [7]. The simulation is stopped if for 2 ps there is no change in the produced defects.

2.2. Potentials

Three empirical embedded atom method (EAM) potentials for *W* are used. There are firstly the one named Finnis–Sinclair (**F**) [2] and its improved version named Ackland–Thetford (**A**) [3], which contains one additional core term in the repulsive pair interaction part for distances smaller than 2.7 Å to improve the compressibility at high pressures. However, both **F** and **A** potentials predict a difference in formation energy for ⟨1 1 0⟩ and ⟨1 1 1⟩ interstitials of 0.7 eV, while the *ab-initio* value is 0.3 eV [9]. The third potential named Derlet–Nguyen–Manh–Dudarev (**D**) [4] provides the correct energies of the interstitials.

For use in collision cascades, the short-range interaction is replaced by the universal potential named Ziegler–Biersack–Littmark (**ZBL**) [1]. Previously [7] we have also tried the Biersack–Ziegler [10] potential, but there was no significant difference in the simulated damage resulting from displacement cacades.

The short and long-range potentials are smoothly connected in such a way that the value of the pair interaction and the one of its first derivative are continuous. The connecting expression is

$$\Psi = \exp(c_0 + c_1 r + c_2 r^2 + c_3 r^3), \quad (1)$$

* Corresponding author.
E-mail address: jan.fikar@psi.ch (J. Fikar).

0022-3115/$ - see front matter © 2008 Elsevier B.V. All rights reserved.
doi:10.1016/j.jnucmat.2008.12.068

where r is the distance between atoms and the coefficients c_0–c_3 are determined by fitting the long range and short-range parts at fixed cutting points r_1 and r_2, which are chosen to be 1.0 Å and 2.2 Å, respectively. The cutting point r_1 is smaller than the value of around 1.5 Å we chose in our previous work [7] in order to significantly improve the smoothness of the fit for the potentials **F** and **A**. The potential **D** can also be smoothly fitted with those cutting points, but unfortunately the resulting displacement threshold of 70 eV is too high, as it should be about 50 eV [12]. In order to improve it, new cutting points for the **D** potential are devised, at 0.8 Å and 1.34 Å, respectively, giving a threshold of about 45 and 61 eV, respectively. The value of 1.34 Å gives intentionally equal first derivatives of the **D** and **ZBL** potentials, thus providing a smoother fit.

The electronic density function is truncated for smaller distances as already described in [7]. At distances shorter than r_1 the electronic density is a constant $\rho_{\max}$ and between r_1 and r_2 we use a connecting formula in the following form:

$$\rho = b_0 + b_1 r + b_2 r^2, \tag{2}$$

where b_0–b_2 are fitted so that the density function and its first derivatives are continuous. This truncation should ensure that for distances smaller than r_1 the forces are only due to the universal potential. It should be remembered that in the EAM of the Finnis type the total potential energy E_i of an atom i surrounded by atoms j is given by

$$E_i = \frac{1}{2}\sum_j V_{ij} - \sqrt{\sum_j \rho_{ij}}, \tag{3}$$

where V_{ij} is the pair-interaction term and ρ_{ij} is the contribution of the electronic density of atom j on atom i, both terms being selected empirically. It shows that the embedded term at short distance is still calculated, hence the truncation alone is not sufficient as for short distances the potential energy is lower than the one predicted by the universal potential by a value of $\sqrt{\rho_{max}}$ This problem is not very important for EAM potentials having small electronic density function at short distances, e.g. for the **F** and **A** potentials, but may be crucial for potentials with a large electronic density as the **D** potential. Indeed, because of the intrinsic empirical nature of these potentials, there is freedom in the choice of the embedded term, which can be compensated by the repulsive pair term to provide an appropriate fit to selected properties of the material. This arbitrary choice makes the comparison of different EAM potentials more difficult. We propose two possible solutions. The first one denoted **I** is to shift the universal potential by

$$\mathbf{ZBL}_{shift} = +\sqrt{\rho_{max}}. \tag{4}$$

The potential energy of a pair of free atoms, a dimer, will then be correct for distances smaller than r_1. In the second one, denoted **II**, we do not consider free atoms but instead one atom is in a perfect BCC lattice and a second free atom is approaching it. Then the shift of the universal potential should be

$$\mathbf{ZBL}_{shift} = +\sqrt{\rho_{max} + \rho_{BCC}} - \sqrt{\rho_{BCC}} \tag{5}$$

in order to recover the correct potential energy at short distances. The ρ_{BCC} is the value of the background electronic density for an atom in a perfect BCC lattice.

The corrections are negligible in case of the **F** and **A** potentials, noting that the embedding term and the electron density function is the same for both potentials, where the universal potential fit is shifted by 5.19 eV and 0.90 eV in solution **I** and **II**, respectively, while for the **D** potential they are more important, with shifts of 60.35 eV and 50.47 eV, respectively. All fitted parameters are summarized in Table 1.

Table 2
Comparison of the vacancy, ⟨1 1 1⟩ dumbbell and ⟨1 1 0⟩ dumbbell formation and migration energies for the **F**, **A** and **D** potentials.

Potential	E^f_v (eV)	E^f_{111} (eV)	E^f_{110} (eV)	E^m_{111} (MeV)	E^m_v (eV)
F	3.631	7.810	8.441	30.7	1.442
A	3.632	8.889	9.613	26.7	1.449
D	3.557	9.476	9.771	61	2.054

3. Results

3.1. Displacement thresholds

The displacement thresholds calculation is based on the method presented in [11]. However, fixed PKA directions are used, namely ⟨1 0 0⟩, ⟨1 1 0⟩ and ⟨1 1 1⟩, and the seed for the random number generator used for calculating the initial Maxwell-distributed velocities of the atoms at temperature of 10 K is changed at every occurrence. The small differences in atom positions in the sample in the moment of initiation of the PKA should have the same effect as the small random changes in the PKA directions as used in [11]. The system is then cooled down and Frenkel pairs are analyzed. PKA energy is increased from 40 eV with a step of 2 eV and at least 10 random seed values for each PKA energy are used. The minimum threshold is found in the ⟨1 0 0⟩ direction. The results are summarized in Table 1. The experimental value is 50.5 ± 1 eV [12].

A variation of the cutting points r_1 and r_2 for the fit of the **D** potential between 0.1 and 1.2 Å and 1.04 and 1.64 Å, respectively, yields the same displacement thresholds. Increasing the cutting points beyond those values increases the displacement threshold. It appears then that the displacement threshold is governed mainly by the long-range part.

3.2. Point defects

Point defect formation and migration energies calculated in a sample of half a million atoms are summarized in Table 2. The

Table 1
The fitted coefficients b and c for different potentials together with cutting points r_1, r_2, shifts of the universal potential and calculated displacement thresholds.

Potential	r_1 (Å)	r_2 (Å)	b_0 (eV^2)	b_1 (eV^2 Å^{-1})	b_2 (eV^2 Å^{-2})	$\rho_{\max}$ (eV^2)
F, A	1.00	2.20	20.310 555	13.187 521	−6.593 761	26.904 316
D	0.80	1.34	610.906 512	7578.149 368	−4736.343 355	3642.166 260
Potential	c_0	c_1 (Å^{-1})	c_2 (Å^{-2})	c_3 (Å^{-3})	$\mathbf{ZBL}_{shift}$ (eV)	Ed (eV)
F.I	11.199 517	−5.964 926	1.022 769	−0.168 289	5.186 937	45
F.II	11.364 142	−6.311 414	1.235 717	−0.208 956	0.981 816	45
A.I	13.034 079	−10.385 873	4.360 975	−0.920 110	5.186 937	61
A.II	13.198 705	−10.732 360	4.573 923	−0.960 777	0.981 816	61
D.I	12.665 511	−9.355 569	3.165 690	−0.252 553	60.350 363	55
D.II	12.964 293	−10.239 391	3.985 637	−0.496 414	50.474 200	55

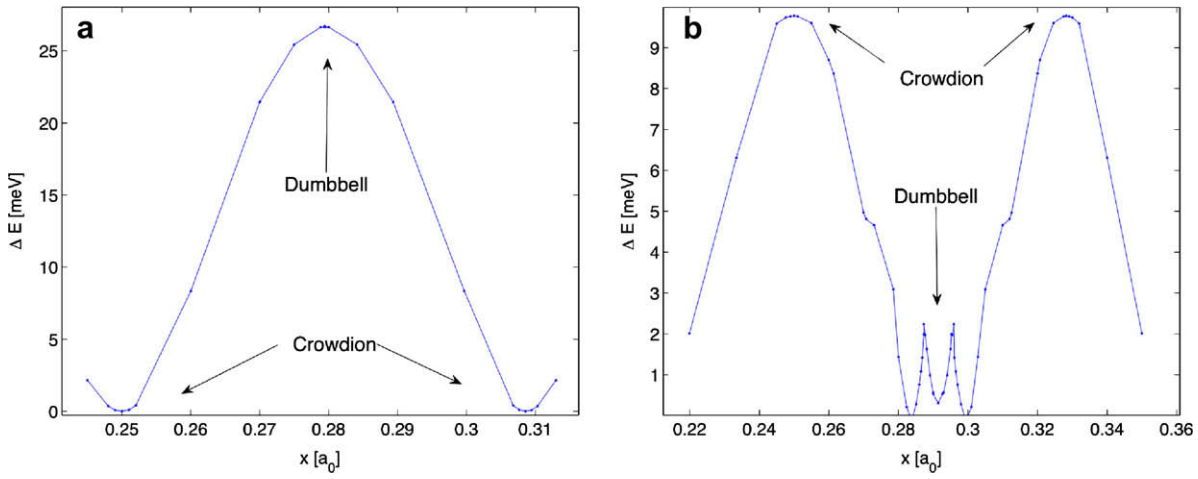

Fig. 1. Static migration energy profiles for the ⟨1 1 1⟩ interstitial in the 1 1 1 direction. (a) Potential A and (b) potential D.

⟨1 1 1⟩ migration energy for **A** corresponds well to the potential barrier of 26.7 MeV in the ⟨1 1 1⟩ direction determined by static calculation [3] (see Fig. 1a). It is not the case for **D**, as the static calculation yields only 9.8 MeV (see Fig. 1b). It appears that there are curious singularities in the potential along ⟨1 1 1⟩, which do not seem to have been explicitly introduced in the design of potential **D** [4], which result in a ⟨1 1 1⟩ interstitial movement slightly deviated from the exact ⟨1 1 1⟩ direction. The mean square displacement of a single ⟨1 1 1⟩ interstitial in a box of 119,000 atoms followed for 5 ns for temperatures between 100 and 300 K and for 1 ns for temperatures between 400 and 1200 K is presented in the Arrhenius plot in Fig. 2. During the observation time at least hundred jumps of the interstitial are seen at the lowest temperature of 100 K. The resulting migration energy for the **D** potential is 48 ± 10 MeV, while for the **A** potential it is 23 ± 6 MeV. Note that the experimental value is 54 ± 5 MeV [9]. The observed migration is 1-D at low temperature and at temperatures of 850 K and 575 K the migration starts to be 3-D for the **A** and **D** potentials, respectively. The observed lower transition temperature for **D** is a result of the lower formation energy of the ⟨1 1 0⟩ interstitial, which is an intermediate state in the ⟨1 1 1⟩ interstitial direction change. The 3-D nature of the migration does not affect the Arrhenius plot much at high temperatures as the change of direction rarely occurs.

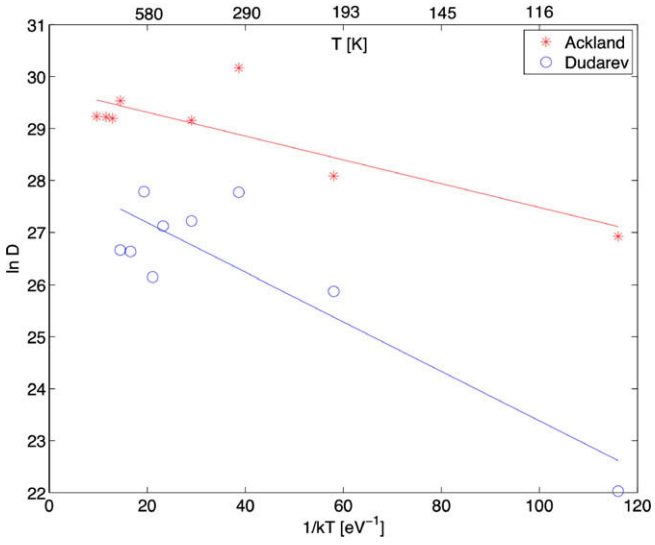

Fig. 2. Arrhenius plot for 1-D migration of the ⟨1 1 1⟩ interstitial in the 1 1 1 direction for the potentials **A** and **D**. The corresponding migration energies are 23 ± 6 MeV and 48 ± 10 MeV for the potentials **A** and **D**, respectively.

3.3. Thermal expansion and temperature of melting

The thermal expansion is shown in Fig. 3. Note the negative thermal expansion with the **D** potential. The experimental thermal expansion is around 4.5×10^{-3} at 1000 K. At this temperature it is close to the one obtained with the **A** potential. For the determination of the melting point, an amorphous sphere is introduced inside a cubic box and the interface between amorphous and crystalline phase is observed for 10 ps at various temperatures. In this manner the conditions in the liquid cascade core during the thermal spike are simulated. The boundary conditions can be constant volume as in cascades or zero pressure to compare with the experimental melting point of tungsten, which is 3695 K. Results are summarized in Table 3.

3.4. Cascades

Collision cascades were simulated at 10 K and 523 K and for a PKA energy of 10, 20 and 50 keV and a PKA direction ⟨1 2 2⟩, ⟨1 3 3⟩,

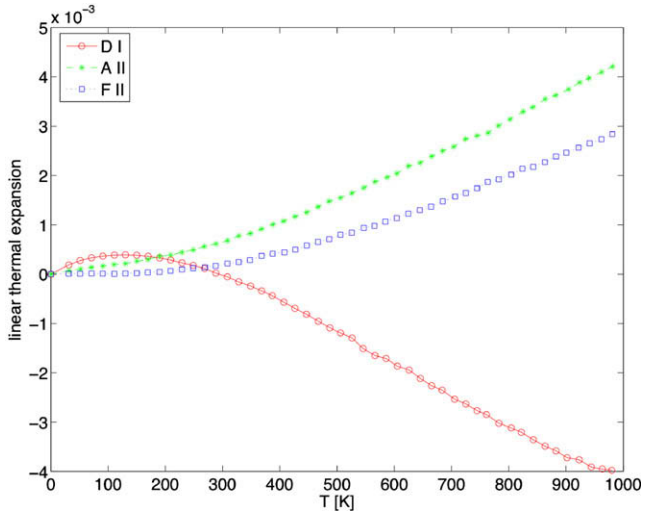

Fig. 3. Linear thermal expansion of the potentials **F**, **A** and **D**.

⟨1 3 5⟩ and ⟨2 3 5⟩. The statistical results are summarized in Tables 4–7. In each case at least 20 simulations with different random seed number are performed and averaged. The numbers of defects produced with the different potentials agree within the statistical errors. It seems thus that the number of defects at high PKA energies does not depend on the displacement threshold energy.

The spatial distribution of vacancies also seems to be similar for all the potentials, although one would expect higher volume per vacancy and lower vacancy in clusters ration in the **D** potential due to its lower melting point and thus larger melted cascade core. This effect can be partially seen at 50 keV, where also slightly more Frenkel pairs are created. The effect might be better seen at higher PKA energies or higher temperatures. Note that the anomalous negative pressure in the **D** potential should be accounted for in this interpretation.

On the other hand, interstitials are found further away from the cascade core for the potentials **F** and **A**, which results in a higher volume per interstitial and lower clustering percentage of interstitials. This effect is due to the lower migration energy of the ⟨1 1 1⟩ interstitials for those potentials, allowing for their rapid escape away from the cascade core.

Table 3
Temperatures of melting for the potentials **A** and **D** with constant volume and zero pressure boundary conditions.

Potential	T_m (K) V = const	T_m (K) $p = 0$
A	6400–6450	5150–5250
D	4500	3750

Table 4
Statistical cascade results for 10 keV, 10 K. *Vac* is the number of produced Frenkel pairs. V_{vac} and V_{int} is the average volume occupied by one vacancy or interstitial, respectively. *Vac in cl.* and *int in cl.* is the proportion of vacancies or interstitials in clusters.

Potential	*vac*	V_{vac} (Å^3)	V_{int} (Å^3)	*vac in cl.* (%)	*int in cl.* (%)
F II	11.6 ± 0.8	3.8 ± 1.1	15.1 ± 4.2	33 ± 4	31 ± 8
A II	9.8 ± 0.8	4.1 ± 1.1	13.2 ± 3.8	27 ± 7	25 ± 9
D I	9.8 ± 0.6	4.9 ± 0.6	10.8 ± 2.2	19 ± 4	52 ± 5
D II	9.5 ± 0.4	4.2 ± 0.4	8.7 ± 1.9	22 ± 3	53 ± 4

Table 5
Statistical cascade results for 10 keV, 523 K. *Vac* is the number of produced Frenkel pairs. V_{vac} and V_{int} is the average volume occupied by one vacancy or interstitial, respectively. *Vac in cl.* and *int in cl.* is the proportion of vacancies or interstitials in clusters.

Potential	*vac*	V_{vac} (Å^3)	V_{int} (Å^3)	*vac in cl.* (%)	*int in cl.* (%)
F II	9.7 ± 0.7	4.6 ± 0.8	48.5 ± 8.2	32 ± 7	19 ± 6
D I	6.8 ± 1.6	4.5 ± 1.3	11.3 ± 7.0	17 ± 12	58 ± 8

Table 6
Statistical cascade results for 20 keV, 10 K. *Vac* is the number of produced Frenkel pairs. V_{vac} and V_{int} is the average volume occupied by one vacancy or interstitial, respectively. *Vac in cl.* and *int in cl.* is the proportion of vacancies or interstitials in clusters.

Potential	*vac*	V_{vac} (Å^3)	V_{int} (Å^3)	*vac in cl.* (%)	*int in cl.* (%)
F	18.9 ± 1.6	10.2 ± 2.9	21.3 ± 2.1	25 ± 5	29 ± 4
F I	18.0 ± 0.9	5.5 ± 0.8	21.1 ± 2.0	27 ± 3	27 ± 3
F II	20.8 ± 0.9	5.6 ± 0.7	18.6 ± 1.8	31 ± 2	31 ± 3
A	15.6 ± 0.9	8.1 ± 2.0	20.9 ± 5.7	23 ± 4	35 ± 6
A I	16.2 ± 0.8	5.6 ± 0.8	19.7 ± 2.5	26 ± 5	30 ± 5
A II	16.3 ± 0.9	7.5 ± 1.7	18.2 ± 3.3	26 ± 4	30 ± 6
D I	17.4 ± 1.0	11.5 ± 1.4	16.6 ± 3.0	18 ± 3	61 ± 4
D II	17.8 ± 0.9	8.7 ± 1.4	11.5 ± 2.2	17 ± 3	64 ± 3

Table 7
Statistical cascade results for 50 keV, 10 K. *Vac* is the number of produced Frenkel pairs. V_{vac} and V_{int} is the average volume occupied by one vacancy or interstitial, respectively. *Vac in cl.* and *int in cl.* is the proportion of vacancies or interstitials in clusters.

Potential	*vac*	V_{vac} (Å^3)	V_{int} (Å^3)	*vac in cl.* (%)	*int in cl.* (%)
F I	49.6 ± 2.8	7.8 ± 1.8	18.3 ± 1.5	44 ± 3	45 ± 4
F II	49.1 ± 2.4	8.4 ± 3.9	20.4 ± 3.5	45 ± 3	48 ± 4
A I	43.7 ± 1.6	9.8 ± 2.5	18.8 ± 2.3	38 ± 3	54 ± 3
A II	41.6 ± 2.4	19.8 ± 5.6	28.5 ± 5.8	34 ± 3	47 ± 4
D I	65.2 ± 4.8	10.5 ± 1.9	10.3 ± 1.9	29 ± 2	82 ± 2
D II	67.1 ± 5.1	24.9 ± 9.5	16.5 ± 4.8	29 ± 3	80 ± 2

4. Conclusions

The investigated potentials produce similar results of collision cascades even though their displacement thresholds are different. A substantial difference in the spatial distribution of interstitials is, however, found. They are diffusing further away from the cascade core with the potentials **F** and **A** relative to results obtained with the **D** potential. It is attributed to the lower migration energy of interstitial obtained with the **F** and **A** potentials. These potentials also predict a too high melting temperature and a too high formation energy of the ⟨1 1 0⟩ interstitial. While the **D** potential is more appropriate there, it yields a negative thermal expansion. We did not observe any important impact of these effects on collision cascades; probably even higher PKA energies or higher temperatures are needed.

A new approach for connecting any general EAM potential to the universal potential is presented. The method overcomes the problematic arbitrary choice of the embedding term, which is compensated at long distances with the pair interaction terms. However, we also compensate it for short distances where the universal potential governs the pair interaction and in this way we are able to obtain potentials that are better comparable to each other. The two proposed corrections **I** (dimer case) and **II** (perfect BCC case) give very similar results for the studied tungsten potentials as the electronic densities of those potentials produce similar shifts of the universal potential.

A different approach is to shift the universal potential by a fitted value to exactly recover the experimental displacement thresholds [11], but contrary to the present method the shifts are mainly negative. It seems that at least for the potential **D** and the chosen cutting points the displacement threshold is due to the long-range part itself, which may be refined to match experimental values.

Acknowledgements

This work has been performed within the framework of the Integrated European Project "ExtreMat" (contract NMP-CT-2004-500253) with financial support by the European Community. It only reflects the view of the authors and the European Community is not liable for any use of the information contained therein. The authors wish to thank C. Björkas for helpful discussions about the displacement threshold. Fruitful discussions with Prof. V. Vitek on empirical potentials are highly appreciated. The Paul Scherrer Institute is acknowledged for the overall use of the facilities.

References

[1] J.F. Ziegler, J.P. Biersack, U. Littmark, The Stopping and Range of Ions in Solids, Pergamon, 1985. p. 41.
[2] M.W. Finnis, J.E. Sinclair, Phil. Mag. A 50 (1984) 45.

[3] G.J. Ackland, R. Thetford, Phil. Mag. A 56 (1987) 15.
[4] P.M. Derlet, D. Nguyen-Manh, S.L. Dudarev, Phys. Rev. B 76 (2007) 054107.
[5] P. Gumbsch, J. Reiedle, A. Hartmaier, H.F. Fischmeister, Science 282 (1998) 1293.
[6] M.J. Caturla, T.D. De la Rubia, M. Victoria, R.K. Corzine, M.R. James, G.A. Greene, J. Nucl. Mater. 296 (2001) 90.
[7] J. Fikar, R. Schaeublin, Nucl. Instrum. and Meth. B 255 (2007) 27.
[8] T.D. De la Rubia, M.W. Guinan, J. Nucl. Mater. 174 (1990) 151.
[9] D. Nguyen-Manh, A.P. Horsfield, S.L. Dudarev, Phys. Rev. B 73 (2006) 020101.
[10] J.P. Biersack, J.F. Ziegler, Nucl. Instrum. and Meth. 194 (1982) 93.
[11] C. Björkas, K. Nordlund, Nucl. Instrum. and Meth. B 259 (2007) 853.
[12] P. Vajda, M. Biget, A. Lucasson, P. Lucasson, J. Phys. F 7 (1977) L123.